Pol. J. Environ. Stud. Vol. XX, No. X (XXXX), 1-15
DOI: *10.15244/pjoes/196742* ONLINE PUBLICATION DATE: 2025-03-10

Original Research

Spatial Scale Effects of 2D and 3D Urban Landscape Pattern on Atmospheric Particulate Matter and Their Seasonal Changes

Haiou Yang[1, 2], Qingming Leng[3○]*, Yanfang Xiao[1]

[1]School of Tourism and Geography, Jiujiang University, Jiujiang 332005, China
[2]Jiangxi Yangtze River Economic Zone Research Institute, Jiujiang University, Jiujiang 332005, China
[3]School of Resources and Environment, Jiujiang University, Jiujiang 332005, China

Received: 4 September 2024
Accepted: 2 December 2024

Abstract

The urban landscape pattern has critical effects on atmospheric particulate matter (PM) pollution. However, the effects may greatly differ with variations of the spatial scales and seasons, which remains poorly understood. This study established a multiple spatial scale analysis on the impact of the urban landscape pattern on PM pollution across different seasons in Nanchang, China, via regular and redundancy analysis (RDA). Six 2D and six 3D metrics were employed to characterize the landscape pattern with buffer radii of 100, 300, 600, 900, 1,200, 2,400, and 4,800 m centered at monitoring stations. Results showed that the effects of the urban landscape pattern on PM pollution have significant seasonal differences and spatial scale effects. Urban landscape pattern has a stronger influence on PM pollution in fall and winter than in spring and summer. The explanatory ability of selected metrics on PM concentrations first increased, then decreased, and finally increased as the scales increased, and the highest accumulated explanatory ability was observed at the 900 m scale. At smaller scales (buffer radii ≤ 900 m), the ability of 3D metrics was stronger than 2D metrics to explain the PM changes, and at larger scales (buffer radii ≥ 1,200 m), the 2D metrics were more explanatory. Percentage of building landscape (PLAND) and patch cohesion index (COHESION) were the key 2D metrics affecting PM pollution, and spatial congestion degree (SCD) and landscape enclosing degree (LED) were the key 3D metrics. The results provide important implications in urban planning for effective PM pollution mitigation.

Keywords: urban landscape pattern, PM pollution, scale effects, 2D and 3D metrics, seasonal changes

Introduction

The rapid urbanization of China in the past decades has brought great economic prosperity, and people's living standards have been significantly improved. However, along with large numbers of people migrating into the urban areas, the cities have suffered from

*e-mail: qingming_leng@jju.edu.cn
Tel.: +86-1817-290-9623
°ORCID iD: 0000-0002-9395-5863

various urbanization-induced ecological environment problems, e.g., air pollution, resource shortages, and traffic congestion. Air pollution, which is one of the leading five pathogenic factors, takes responsibility for more than five million global deaths per year based on the Global Burden of Disease Study in 2019 [1-3]. As a typical air pollutant, inhalable atmospheric particulate matter (PM) would reduce atmospheric visibility and worsen the air quality, subsequently resulting in serious respiratory, pulmonary, and cardiovascular diseases [4, 5]. Since 2013, the Chinese government has announced a variety of measures to control PM pollution, which have stopped the worsening trend of air quality in most cities. However, efforts devoted to further mitigating PM pollution are still urgently needed since $PM_{2.5}$ and PM_{10} concentrations in most cities still exceed the 35 μg/m^3 and 70 μg/m^3 threshold of World Health Organization Interim Target 1 (WHO IT-1).

Numerous studies have shown that the urban landscape pattern, including landscape composition and landscape spatial configuration, has a great impact on PM pollution [6-9]. Generally, different urban landscape components will act as the pollution source or pollution sink to increase or decrease the PM concentrations directly. For instance, the higher the percentage of impermeable surfaces in cities, the more serious the PM pollution, which is like a source component; and the higher the percentage of green-blue space in cities, the better the air quality, which can be regarded as a sink component. The effect of urban landscape spatial configuration on PM pollution may be indirect, referring to urban landscape configuration changing the PM concentrations through altering the local microclimate, including wind speed and direction, temperature, and humidity, which are critical influencing factors for PM pollution transport and dispersion [10]. Therefore, clarifying the "urban landscape pattern-PM pollution" relationship can provide important implications in landscape optimization strategy for effective PM pollution mitigation and sustainable urban development [11, 12].

The impacts of the urban landscape pattern on PM pollution are complex, and their relationship may depend on seasons and spatial scales [6, 7, 12]. The spatial scale refers to different areal extent. In the past decades, research on the "landscape pattern-air pollution" relationship has been conducted on the urban scale [8, 13], urban agglomeration scale [11, 14], and national scale [6, 15]. However, few studies have been conducted on the intra-urban scale [7, 16], and consensus on which spatial scale urban landscape pattern impacts air pollution most has not been reached yet. In particular, most existing studies employ the annual average PM concentrations or PM concentrations at another single time scale when studying the relationship between the urban landscape pattern and PM pollution [17, 18]. Considering significant seasonal variations exist in the PM concentrations, the effects of the urban landscape pattern on PM pollution may also be season-dependent [19].

Early research usually adopted 2D landscape metrics to quantify the urban landscape pattern [20]. With the development of urbanization and aero photography and remote sensing technologies over the years, many 3D metrics have been established from a totally new view or based on traditional 2D metrics and increasingly applied to depict the horizontal and vertical characteristics of urban landscapes [8, 21, 22]. Experiments simulating high-density urban areas through ideal models have verified that 3D urban landscape patterns can exert a significant influence on air pollution [23-25]. However, whether 2D or 3D urban landscape characteristics have a greater impact on air pollution at the urban scale remains controversial. Some studies thought 2D characteristics are the determining factors of anthropogenic activity on air pollution, while others reported that 3D characteristics could better account for air quality variability [17, 22]. Further research is needed to support these conclusions.

Therefore, this study attempted to investigate the associations between 2D/3D landscape patterns and PM pollution at multiple intra-urban scales, and the variation in relationships across four seasons was also explored. Nanchang, a representative city in central China, was chosen as the study area. $PM_{2.5}$ and PM_{10} were adopted as typical PM pollutants. Twelve 2D/3D landscape pattern metrics were extracted from 22 air quality monitoring stations with buffer radii of 100, 300, 600, 900, 1,200, 2,400, and 4,800 m (i.e., buffer scales). The study specifically aimed to: (1) analyze the variability of 2D/3D landscape pattern characteristics at multiple scales in Nanchang; (2) explore the relative importance of 2D and 3D landscape pattern characteristics in PM pollution mitigation; and (3) quantitatively analyze the influence of landscape pattern on PM pollution across different scales and seasons.

Materials and Methods

Study Area

Nanchang, located on the bank of Poyang Lake in central China, is the capital city of Jiangxi Province. Nanchang experiences the subtropical monsoon climate, the average annual precipitation and temperature range of which are 1,600 mm to 1,700 mm and 17°C to 17.7°C. This city has undergone expansive urbanization and has suffered from severe PM pollution in recent years. The proportion of the urban population had grown from 65.71% in 2010 to 75.16% in 2019. Construction has been frequently projected here, and plenty of high buildings have been built, forming the complex 3D landscape pattern. The average annual concentrations of PM_{10} and $PM_{2.5}$ were respectively 116 μg/m^3 and 69 μg/m^3 in 2013. After years of atmospheric environment control, those values declined to 74 μg/m^3 and 36 μg/m^3 in 2019, which

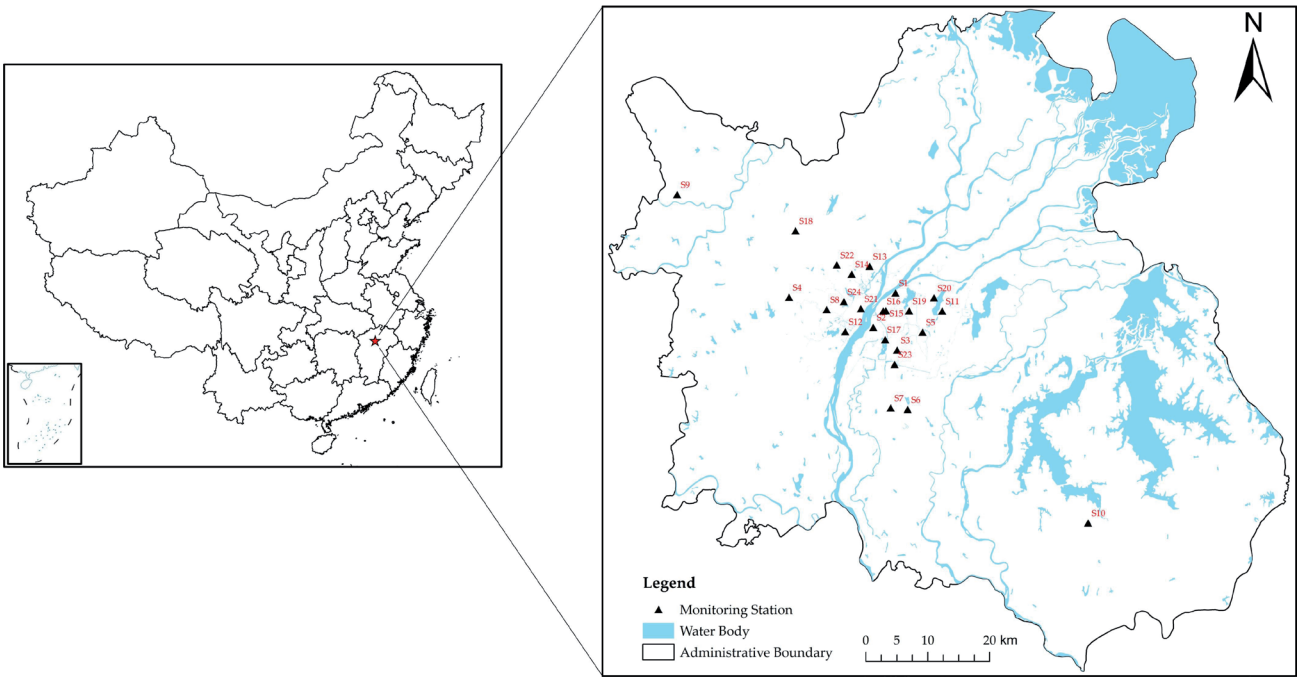

Fig. 1. Distribution of air monitoring stations in Nanchang.

still overstepped Level II of the National Ambient Air Quality Standard (NAAQS) in GB3095–2012 [26]. To record the hourly ground-level data of air pollutants, Nanchang has established 24 air quality monitoring stations, including 9 national and 15 provincial ones (Fig. 1). The recording processes obey the national measurement standards.

Data Acquisition and Processing

Three kinds of data, including PM concentrations, land use, and building information around monitoring stations, were involved in this study:

- PM concentrations data. Daily data in 2019 were acquired from the Nanchang Environmental Monitor Center. A year was split into spring (March to May), summer (June to August), autumn (September to November), and winter (December to February). Monitoring stations with 25 or more records per month (23 records in February) were adopted for the calculation of monthly and seasonal average $PM_{2.5}$ and PM_{10} concentrations. Hence, 22 of the 24 monitoring stations were finally selected because of missing values (S18 and S24 were excluded).
- Land use data. The data at 30 m resolution were obtained from Global Geographic Information Bulletin products (http://www.globallandcover.com/). The study area was divided into 7 land use/land cover types, including farmland, forest land, grassland, wetland, water body, artificial surface, and bare land. The Kappa coefficient and the overall data accuracy were 0.82 and 85.72%, respectively. Based on the landscape information, the 2D landscape pattern metrics could be calculated around the monitoring stations with specific buffer zones by using FRAGSTATS 4.2.
- Building information. The main building information, such as building contour and height, was extracted from the AutoNavi Map (http://lbs.amap.com/) in 2018. Based on the building information, the 3D landscape pattern metrics could be calculated around the monitoring stations with specific buffer zones by using the spatial analysis software ArcGIS10.2.

Calculation of 2D/3D Landscape Pattern Metrics in Circular Buffer Zones

Landscape metrics that condense the composition and configuration information of landscapes are commonly adopted to describe the landscape pattern [27, 28]. Generally, the landscape composition metrics (e.g., percentage of building patch (PLAND)) can directly affect PM pollution [29]; the landscape configuration metrics (e.g., patch density (PD)) can indirectly affect PM pollution by air circulation and air pollutants diffusion [18]. This study measured the landscape pattern with twelve 2D and 3D metrics, the formulas of which are shown in Table 1. These metrics were extracted with buffer radii of 100, 300, 600, 900, 1,200, 2,400, and 4,800 m centered at monitoring stations, and then the relative importance of these metrics in PM concentration mitigation can be analyzed.

2D metrics are the earliest and most widely used metrics that have been used to quantify the landscape pattern [30]. This study employed six 2D metrics, including PLAND, PD, largest patch index (LPI), landscape shape index (LSI), building patch cohesion index (COHESION), and building aggregation index

Table 1. 2D and 3D landscape pattern metrics used in the study.

Class	Variable Name	Abbreviation	Formula	Description
2D	Percentage of building landscape	PLAND	$\frac{\sum_{i=1}^{n} a_i}{A} \times 100\%$	a_i is the area of building patch i, and A is the area of buffer zones (the same as below)
	Patch density	PD	$\frac{n_i}{A} \times 100\%$	n is the number of building patches
	Largest patch index	LPI	$\frac{max(a_i)}{A} \times 100\%$	$max(a_i)$ is the largest a_i in area
	Landscape shape index	LSI	$\frac{E}{minE}$	E is the total length of building landscape edge according to the number of cell surfaces, and $min\ E$ is the shortest E in length
	Patch cohesion index	COHESION	$\left[1 - \frac{\sum_{j=1}^{n} P_{ij}^*}{\sum_{j=1}^{n} P_{ij}^* \sqrt{a_{ij}^*}}\right] * \left[1 - \frac{1}{\sqrt{Z}}\right]^{-1} \times 100\%$	a_{ij}^* is the area of patch ij; P_{ij}^* is the perimeter of patch ij according to the number of cell surfaces; Z is the total number of cells in landscape
	Aggregation index	AI	$\left[\sum_{i=1}^{m} \left(\frac{g_{ii}}{max \rightarrow g_{ii}}\right) P_i\right] \times 100\%$	g_{ii} is the number of like adjacencies and joins between pixels of buildings, and $max \rightarrow g_{ii}$ is the maximum g_{ii} in number
3D	Building average height	BAH	$\frac{1}{n}\sum_{i=1}^{n} H_i$	H_i is the height of building i, and n here is the number of buildings
	Building height range	BHR	$H_{max} - H_{min}$	H_{max} and H_{min} are the maximum and minimum values of H_i in height in the buffer area
	Building average volume	BAV	$\frac{1}{n}\sum_{i=1}^{n} V_i$	V_i is the volume of building i, and volume is the multiplication of footprint and height
	Spatial congestion degree	SCD	$\frac{\sum_{i=1}^{n} V_i}{max\{H_i\} \times A} \times 100\%$	
	Building volume density	BVD	$\frac{1}{A}\sum_{i=1}^{n} V_i$	
	Landscape enclosing degree	LED	$\frac{l_i}{L_i} \times 100\%$	l_i is the length of buildings on the outside of the buffer area, and L_i is the perimeter of the buffer area

(AI), to measure the 2D landscape pattern. The building PLAND can directly affect the PM concentrations. The LSI represents the complexity of urban shape, in which the higher LSI indicates the more complex urban shape. The PD and LPI describe the degree of landscape pattern fragmentation, while AI and COHESION refer to the degree of landscape pattern aggregation. These four metrics may positively or negatively affect the diffusion of air pollutants [31]. FRAGSTATS 4.2 was used for the computation of 2D landscape pattern metrics, and for more software details and metrics sources, see the FRAGSTATS user manual.

For the selection of 3D metrics, those typical metrics proven to be influential on urban environments [7, 32], including building height range (BHR), building average height (BAH), building average volume (BAV), spatial congestion degree (SCD), building volume density (BVD), and landscape enclosing degree (LED), were employed in this study. Among these 3D metrics, building height-related metrics are the most widely used and can greatly affect the wind field in urban canopy [33]. Building density-related metrics (e.g., BVD, SCD, and LED) have a substantial effect on the heat capacity and wind field of urban environments, as well as on air pollutant transportation. The BAV reflects the building volume, energy consumption, and so on, and it may also influence the PM concentrations through temperature and wind change. Notably, the commonly used sky view factor (SVF) that regulates the incoming ventilation and solar energy from the canopy layer [34] was not chosen due to data inaccessibility. All the 3D metrics were obtained with the spatial analysis software ArcGIS10.2.

Statistical Analysis

Several statistical analysis methods were employed in the study. First, the Kolmogorov–Smirnov (K-S) test was used to test the normality of $PM_{2.5}$/PM_{10} concentrations in each monitoring station. Then, the independent sample t-test was adopted to test the seasonal variations in $PM_{2.5}$/PM_{10} concentrations among different monitoring stations. The one-way analysis of variance (ANOVA) was adopted to determine the $PM_{2.5}$/PM_{10} differences among 22 monitoring stations. Redundancy analysis (RDA) is a method generally used to study the relationship between landscape metrics and environmental factors. RDA assumes that the relationship between the explanatory variables and explained variables is linear and can be regarded as an extension of principal analysis since the canonical ordination vectors are linear combinations of the explanatory variables. In the RDA biplots, the arrows represent the explanatory variables and explained variables. If the arrows of two variables point in the same direction, the relationship between them is positive, and the angle between the two variable arrows is inversely proportional to the degree of their relationship. The length of the arrow can be regarded as a mutual similarity of contributions [35, 36]. Before employing RDA, the detrended correspondence analysis (DCA) was utilized to analyze the PM data. In this study, the DCA results showed that the longest gradient of the four ordination axes was all less than 3, confirming the suitability of the linear RDA model. The RDA operation was performed twice to avoid collinearity among landscape pattern metrics. The regular analysis was operated on SPSS 21.0 (IBM Company, USA), and the RDA analysis was performed on CANOCO 5.0 (Microcomputer Power Company, USA).

Results

Spatial and Seasonal Variation of PM Pollution

The independent sample t-test ($p<0.01$) showed that PM pollution had evident seasonal variations in most seasons, except for PM_{10} in spring and autumn (Table 2). Suitable t-test results were selected according to the homogeneity of variance. The boxplots further exhibited consistent seasonal variations, in which summer observed the lowest concentrations, whereas winter observed the highest ones (Fig. 2). PM pollution in winter was more severe than in other seasons, in which the average $PM_{2.5}$ and PM_{10} concentrations reached 51.44 and 85.33 μg/m^3, respectively. The values in other seasons were 37.37 and 86.09 μg/m^3 in autumn, 35.49 and 77.71 μg/m^3 in spring, and 22.12 and 54.70 μg/m^3 in summer.

The one-way ANOVA showed that PM pollution had noticeable spatial changes across all seasons ($p<0.05$). The core areas generally had higher seasonally mean concentrations than the perimeter zones. The highest $PM_{2.5}$ concentration was observed at S3 (71.52 μg/m^3) and PM_{10} concentration at S7 (111.91 μg/m^3) in winter; the lowest $PM_{2.5}$ concentration was observed at S10 (10.17 μg/m^3) and PM_{10} concentration at S19 (35.25 μg/m^3) in summer. For all the monitoring stations in four seasons, PM concentrations overtopped the NAAQS Level I, which was set at 15 μg/m^3 for $PM_{2.5}$ and 40 μg/m^3 for PM_{10}. In all seasons except summer, the PM

Table 2. Seasonal differences of PM pollution via the independent sample t-test.

Variables	Seasons	Levene's test for the equation of variance		Suitable t-test results		
		F	p	t	df	p
$PM_{2.5}$	Spring-summer	252.77	0.00	29.34	3421.18	0.00
	Spring-autumn	17.52	0.00	-3.66	3906.35	0.00
	Spring-winter	441.48	0.00	-21.45	3155.04	0.00
	Summer-autumn	154.60	0.00	-36.18	3627.19	0.00
	Summer-winter	1173.53	0.00	-42.85	2501.38	0.00
	Autumn-winter	619.51	0.00	-19.47	2938.61	0.00
PM_{10}	Spring-summer	291.74	0.00	26.64	3534.28	0.00
	Spring-autumn	0.71	0.40	-7.88	3949.65	0.00
	Spring-winter	338.66	0.00	-5.67	3286.52	0.00
	Summer-autumn	183.75	0.00	-34.27	3384.90	0.00
	Summer-winter	1053.31	0.00	-25.26	2649.56	0.00
	Autumn-winter	308.28	0.00	0.61	3441.14	0.54

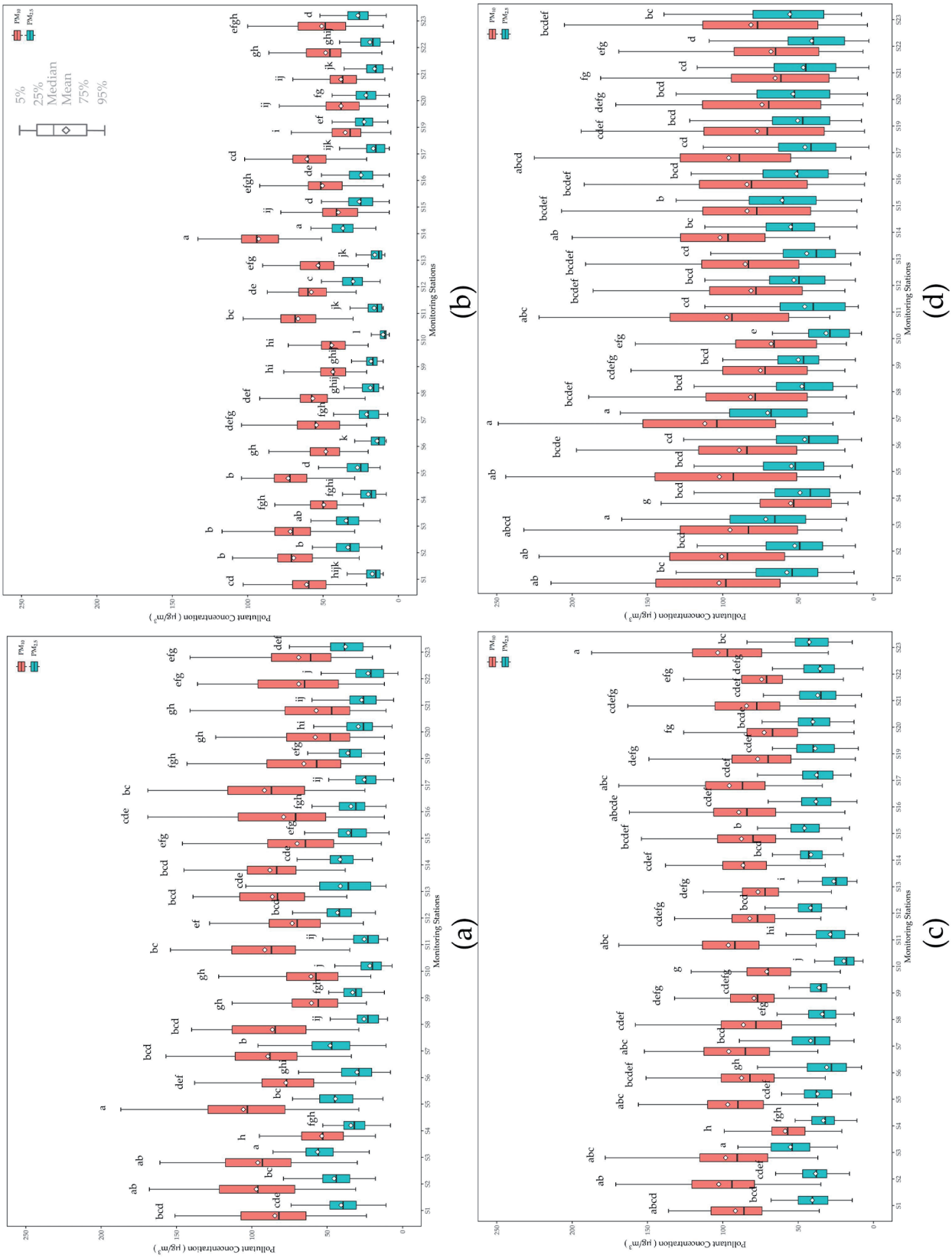

Fig. 2. Boxplots for $PM_{2.5}$ and PM_{10} of the monitoring stations in Nanchang in 2019: a) Spring; b) Summer; c) Autumn; d) Winter.

pollution exceeded the NAAQS Level II, which was set at 35 μg/m^3 for $PM_{2.5}$ and 70 μg/m^3 for PM_{10}.

Differences in Landscape Pattern Metrics within Distinct Buffer Scales

The spatial variability of 2D metrics at distinct buffer scales around the monitoring stations is shown in Fig. 3. The PLAND located in central areas were generally larger than those in perimeter zones. Most of the maximum PLANDs were observed at the 100 m scale. PLAND varied slightly within the 600 m radius and decreased with the increase in scales when the radius was higher than 600 m (Fig. 3a)). Likewise, the LPI values in central areas were larger than those in perimeter zones, the values decreased with the increase in scales (Fig. 3c)). The PD and LSI showed greater scale effect than other metrics. The PD declined quickly with the rise in scales, and its value at the 100 m scale was apparently greater than that at the other scales (Fig. 3b)). Inversely, the LSI increased rapidly with the increase in scales, and the maximum LSI was found at the 4,800 m scale (Fig. 3d)). The spatial variability degrees of COHESION and AI were small, and their scale effects were insignificant (Fig. 3c) and 3d)).

All the 3D landscape pattern metrics at different buffer scales around the 22 monitoring stations showed an obvious spatial differentiation from the center to the outside (Fig. 4). BAH, SCD, BVD, and LED had the largest spatial variability. The maximum values were always observed in central areas, whereas low values were observed in perimeter zones. The spatial variability of BAV was lower than that of BAH, SCD, BVD, and LED, and BHR had the least spatial variability. All the 3D landscape pattern metrics presented obvious spatial scale effects. BHR increased with the increase in scales (Fig. 4b)). For most of the monitoring stations, the maximum BHR was observed at the 4,800 m scale. Conversely, SCD decreased with the increase in scales (Fig. 4d)), and the maximum SCD (i.e., 22%) was observed at the 100 m scale around S19. BAH and BAV had similar scale effects, and these parameters increased with the increase in scales when the buffer zones radii ≤ 600 m and decreased with the increase in scales when the buffer zones radii ≥ 900 m. The maximum BAH of 108 m and maximum BAV of 98,521 m^3 were observed at the 100 m scale around S14. For most of the monitoring stations, LED and BVD increased as the buffer radii increased when radii ≤ 900 m, while they decreased when radii ≥ 1,200 m.

Effects of Landscape Pattern Metrics on PM Pollution

The RDA results showed the effects of landscape pattern metrics on PM pollution at distinct buffer scales in four seasons (Table 3 and Fig. 5). At most scales, the selected metrics explained that autumn and winter had higher PM variations than spring and summer. In winter, when there were the highest PM concentrations, the most important explanatory variables were COHESION (36.7%) at 100 m scale, COHESION (21.30%) at 300 m scale, LED (20.50%) at 600 m scale, AI (15.50%) at 900 m scale, PD (19.20%) at 1,200 m scale, PLAND (20.00%) at 2,400 m scale and PLAND (49.60%) at 4,800 m buffer scale, and most of these parameters were 2D landscape pattern metrics. In summer, when there were the lowest PM concentrations, the most important explanatory variables were BAV (32.3%) at 100 m scale, BVD (23.5%) at 300 m scale, LED (28.90%) at 600 m scale, LED (27.3%) at 900 m scale, LPI (20.6%) at 1,200 m scale, BVD (20.7%) at 2,400 m scale and LED (26.6%) at 4,800 m buffer scale (Table 3), and most of these parameters were 3D landscape pattern metrics. It can be concluded that the relative importance of metrics varied with seasons in 2D and 3D perspective. When the PM concentrations were higher, the 2D landscape pattern metrics showed a stronger association with PM concentrations, such as PLAND and COHESION; when the PM concentrations were lower, the 3D landscape pattern metrics showed a stronger association with PM concentrations, such as LED and SCD.

The RDA results also demonstrated obvious spatial differences in the effects of the landscape pattern on PM pollution. The total explanatory ability of 2D/3D metrics exhibited consistent scale variations in four seasons, in which the values first increased, then declined, and finally increased as the scales enlarged. The explanatory values ranged from 79% to 32.4%. The highest accumulated explanatory was found at 900 m scale across four seasons. At 900 m scale, the most significant explanatory variables were SCD (24.7%), LED (27.3%), PD (19.9%), and AI (15.5%) in spring to winter, respectively. At larger scales (2,400 m and 4,800 m scales), the PLAND of 2D landscape pattern metrics was the most important explanatory variable. At smaller scales (100, 300, and 600 m scales), the explanatory ability of 3D metrics such as LED and SCD was greater than that of 2D metrics.

Since the minimum and maximum PM concentrations were observed in summer and winter, the RDA biplots were chosen for further analysis (Fig. 6 and Fig. 7). When PM concentrations were higher or at larger scales, the most important 2D explanatory variable, PLAND, was positively associated with $PM_{2.5}$ and PM_{10} at multiple scales in summer and winter. When PM concentrations were lower or at smaller scales, the most important 3D explanatory variable, LED, was positively associated with $PM_{2.5}$ at all scales in both summer and winter, but it was often negatively associated with PM_{10} in summer. Generally, COHESION was negatively associated with PM concentrations when the PM concentrations are higher in winter, while positively associated with PM concentrations at all scales when the PM concentrations are lower in summer. SCD and BVD were positively associated with $PM_{2.5}$ at all scales in both summer and winter, while negatively associated with PM_{10} at all scales in both summer and winter.

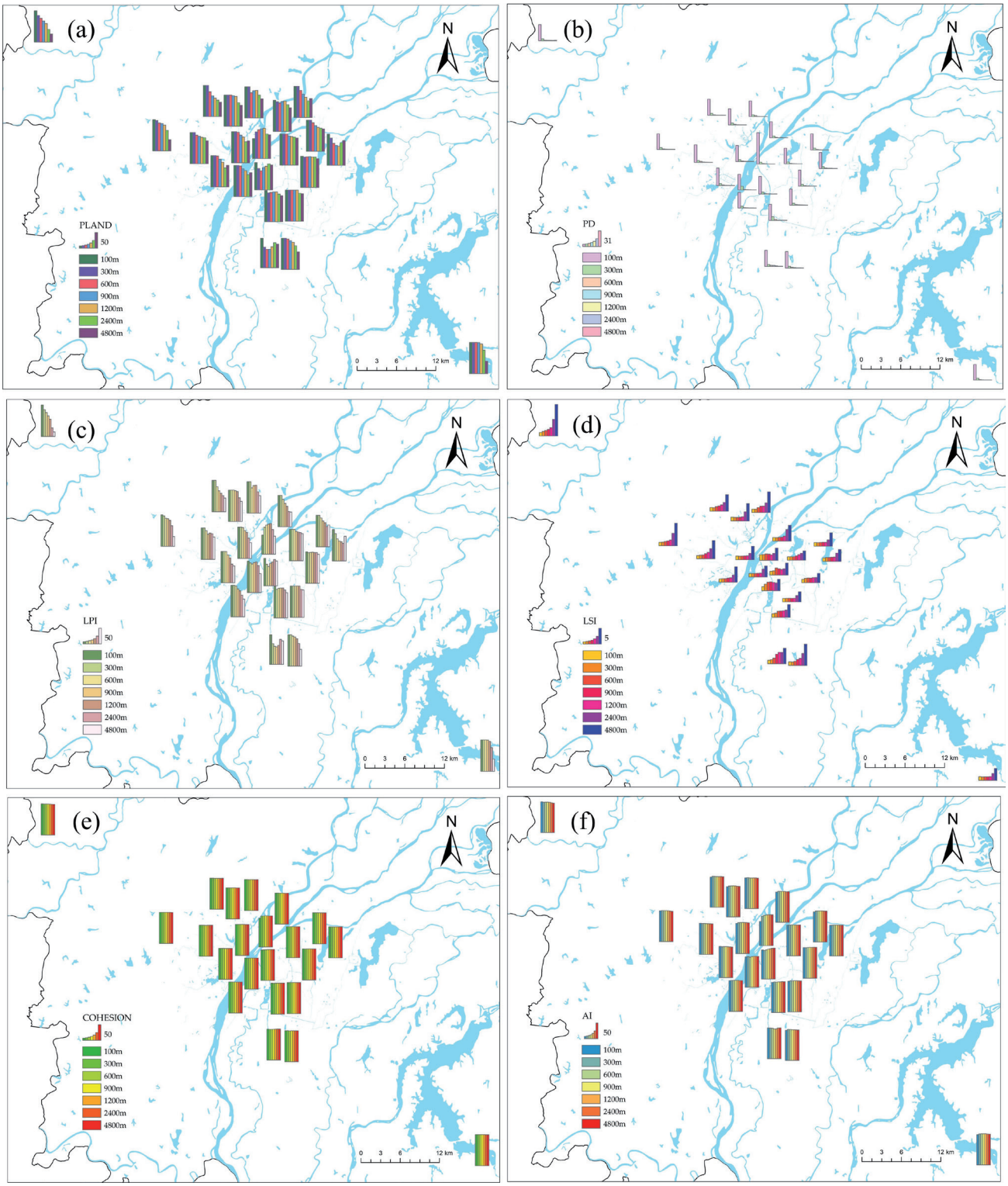

Fig. 3. The 2D landscape pattern metrics with buffer scales of 100, 300, 600, 900, 1,200, 2,400, and 4,800 m around monitoring stations in Nanchang: a) PLAND; b) PD; c) LPI; d) LSI; e) COHESION; and f) AI.

Discussion

Influence of Seasonal Changes

Existing studies have demonstrated that the influence of the urban landscape pattern on air quality varies seasonally [31, 37-39]. Similar observations were found in this work, the selected landscape pattern metrics in autumn and winter explained higher PM variations than that in spring and summer. Distinct meteorological conditions in different seasons may be the crucial factors [19]. Generally, regional precipitation, monsoon, wind, relative humidity, and other meteorological factors can affect the PM concentrations [40, 41]. In spring and

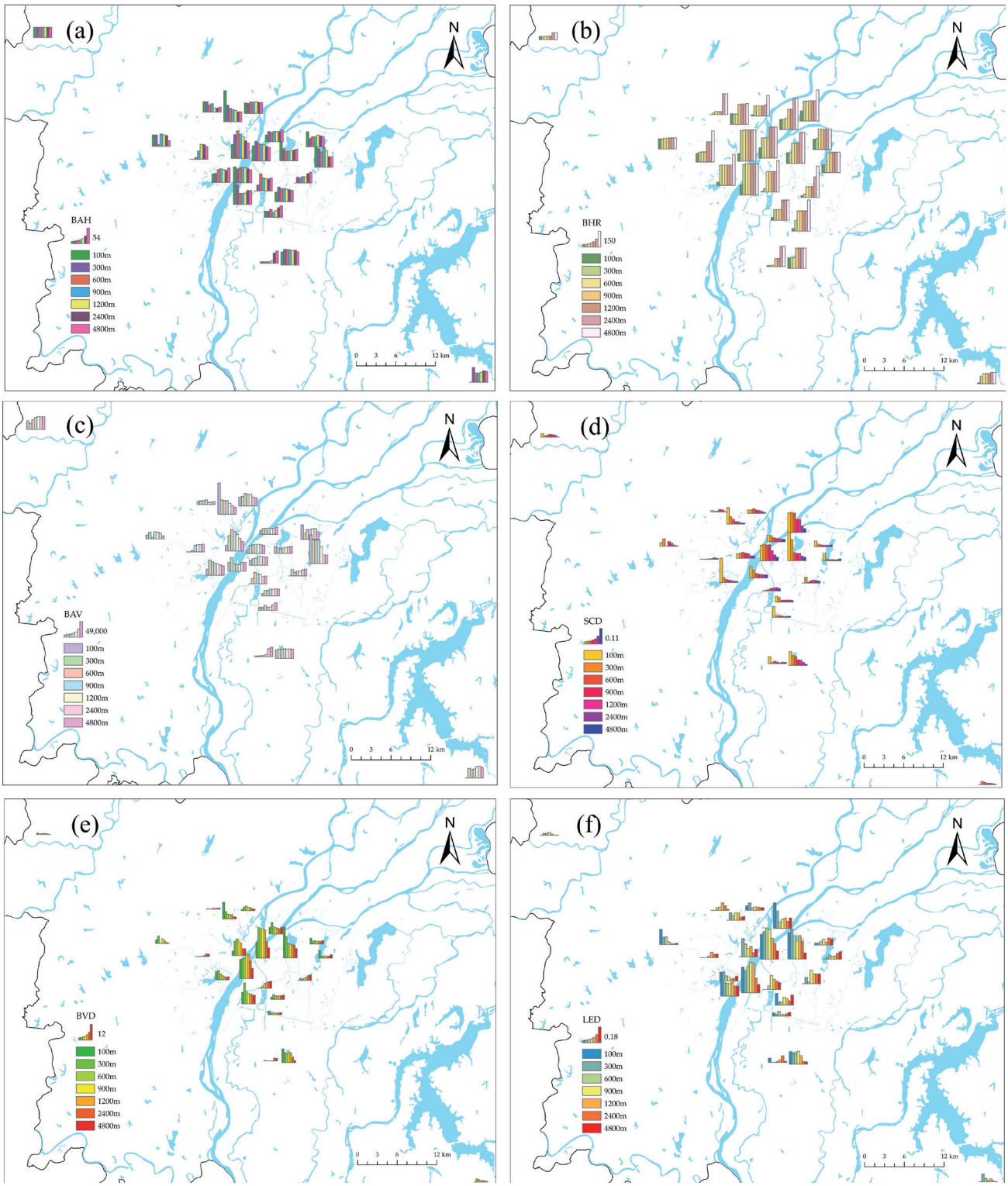

Fig. 4. The 3D landscape pattern metrics with buffer scales of 100, 300, 600, 900, 1,200, 2,400, and 4,800 m around monitoring stations in Nanchang: a) BAH; b) BHR; c) BAV; d) SCD; e) BVD; f) LED.

summer, the strong Asian monsoon in Nanchang results in abundant precipitation, speeding up the airflow and removing air pollutants [42]. In autumn and winter, the dissipation of PM pollution is greatly hindered by the inversion of the temperature gradient, and the low velocity of wind conditions is adverse for the diffusion of air pollutants [43].

Although an agreement about the impact of the urban landscape pattern on PM pollution differs with the season has been reached, controversies still exist. Liu et al. conducted a study of 83 major Chinese cities and found that landscape patterns in spring and summer were more significantly linked with air quality levels than those in fall and winter [31]. Shi et al. studied 279

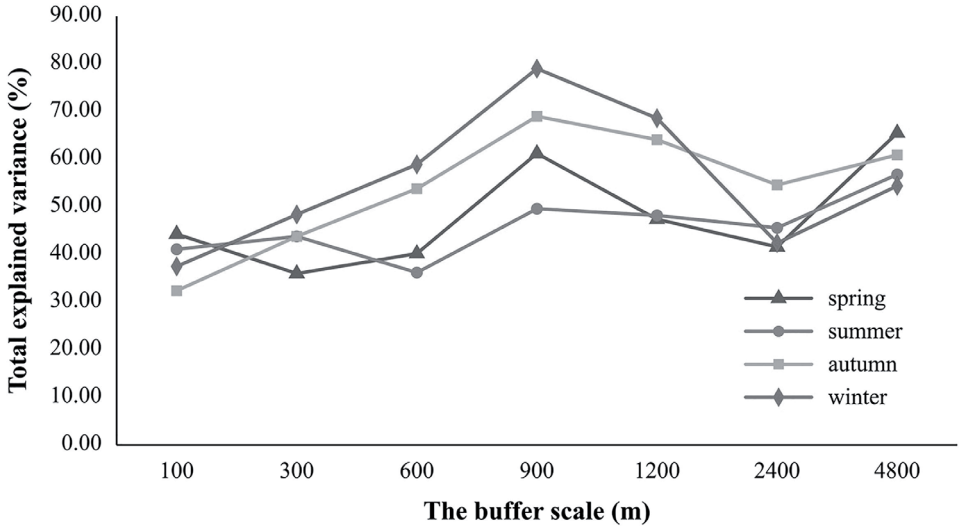

Fig. 5. The explanatory ability of landscape pattern metrics on PM pollution at different buffer scales across four seasons.

Chinese cities and suggested that the results would be more productive if spring and winter data were used instead of summer and autumn data [39]. Cao et al. recommended spring and autumn more than summer and winter, according to their research in Beijing [7]. The result of our study showed autumn and winter explained higher PM variations than spring and summer. These controversies may be attributed to different study areas or PM data. Since the meteorological conditions in summer and winter would greatly affect the PM concentrations, which may weaken the influence of the urban landscape pattern on PM pollution, it is more scientific to study the relationship under relatively consistent macro meteorological conditions. Thus, we insist that the result will be more credible if spring and autumn data are used instead of summer and winter data when exploring the "urban landscape pattern-air pollution" relationship.

Moreover, this study added to the limited literature on seasonal comparisons of the relative importance of landscape pattern metrics on PM concentrations. To the best of our knowledge, Cao et al. probably made the only relevant work. They found that the relationship between landscape pattern and environment depended on the season greatly and that building height indicators were positively associated with $PM_{2.5}$ concentrations only in spring and autumn [7]. Our work presented that the relative importance varied with seasons for 2D and 3D metrics. The 2D metrics, such as PLAND and COHESION, had the stronger explanatory ability in autumn and winter when there were usually high PM concentrations, while the 3D metrics, such as LED and SCD, had the stronger explanatory ability in spring and summer when there were usually low PM concentrations. To sum up, the urban landscape pattern-air pollution relationship has not been well understood when considering seasonal change, and more research should be conducted to explore their relationship further.

Influence of Spatial Scales

Seven buffer radii 100, 300, 600, 900, 1,200, 2,400, and 4,800 m were created to further distinguish the scale effects of landscape pattern on PM concentrations variation, and the setting of buffer scales learned from some representative landscape-related approaches [16, 26, 44-46]. This work demonstrated that the explanatory ability of metrics on PM concentrations tended to first increase, then decline, and finally increase as scales enlarge. The metrics explained that the PM concentration variation was best at the 900 m buffer scale. Previous "landscape pattern–air pollution" relationship works seldom involve the research of scale effects. Shi et al. adopted buffers with radii of 50, 100, 200, 300, 400, and 500 m in Hong Kong but did not refer to the optimal scale [45]. Huang et al. considered a narrow buffer range (25, 50, 75, 100, 150, and 200 m) in Shanghai, and the scale of 100 m was finally determined [16]. The disagreement on an optimal scale is very likely related to the selected landscape pattern metrics since the physical basis of pollution dispersion and diffusion can result in distinct buffer widths of various morphological metrics [46-49].

In comparison with existing studies that examined intra-urban air pollution variability at a single spatial scale or fixed grids with specific resolution [17, 50], the present study showed that the explanatory ability of 2D metrics on PM concentrations was less than that of 3D metrics at small scales (100, 300 and 600 m scales), which were supported by many existing findings. For instance, Ke et al. found that the explanatory ability of 3D landscape pattern metrics outperformed that of the 2D metrics in Hangzhou [17]. Cao et al. found that $PM_{2.5}$ concentrations in Beijing are significantly and positively related with BVD and building height density (BHD) at 100 and 200 m scales but not at the 500 and 1,000 m scales [7]. Although the study areas

Table 3. The RDA results for the percentage of overall PM concentration variation explained by landscape pattern metrics.

Seasons	Scales	Explained variation (%)				Total explained variance (%)	Key landscape pattern metrics (contribution%)
		Axis 1	Axis 2	Axis 3	Axis 4		
Spring	100 m	30.71	13.61	51.66	4.02	44.3	PLAND(32.8), BHR(14.1), COHESION(12.8)
	300 m	26.16	9.81	55.5	8.53	36	PLAND(19.4), BAV(11.7), AI(11.1)
	600 m	34.33	5.84	47.97	11.86	40.2	SCD(27.5), BAV(12.8), LED(11.5)
	900 m	47.73	13.43	34.58	4.26	61.2	SCD(24.7), BAH(13.5), AI(11.4)
	1,200 m	34.05	13.35	47.61	4.99	47.4	BAV(14.7), LED(12.2), BAH(11.3), SCD(10.4)
	2,400 m	37.45	4.13	45.33	13.09	41.6	PLAND(31.8), BHR(16.3), SCD(11.8)
	4,800 m	58.39	7.07	23.32	11.22	65.5	PLAND(43.9), SCD(12)
Summer	100 m	32.72	8.33	55.62	3.33	41.1	BAV(32.3), BVD(18.1)
	300 m	36.03	7.75	51.5	4.72	43.8	BVD(23.5), LED(16.8), BAV(14.3%)
	600 m	29.13	7.1	58.37	5.4	36.2	LED(28.9), LPI(13.5)
	900 m	43.2	6.37	44.84	5.59	49.6	LED(27.3), SCD(18.5)
	1,200 m	37.18	11.04	50.32	1.46	48.2	LPI(20.6), SCD(19.7), LED(14.5)
	2,400 m	38.03	7.58	49.52	4.87	45.6	BVD(20.7), SCD(13.6), PD(12.5)
	4,800 m	49.17	7.63	38.38	4.82	56.8	LED(26.6), PLAND(20.7), SCD(19.6)
Autumn	100 m	27.48	4.91	50.04	17.57	32.4	SCD(24), COHESION(23.8)
	300 m	32.39	11.39	35.96	20.26	43.8	COHESION(25.8), BHR(23.2.), LED(21.3)
	600 m	40.76	13.05	27.6	18.59	53.8	AI(20.2), LSI(13.1), BHR(10.6)
	900 m	52.47	16.54	22.43	8.56	69	PD(19.9), BHR(15.1), BAV(14.8)
	1,200 m	47.66	16.46	20.83	15.05	64.1	BHR(22.1), BAV(21.9)
	2,400 m	44.4	10.18	25.71	19.71	54.6	BHR(30.4), AI(13.9)
	4,800 m	47.27	13.63	22.07	17.03	60.9	PLAND(50.9), COHESION(13.4)
Winter	100m	26.31	11.15	50.82	11.72	37.5	COHESION(36.7), PLAND(20.3)
	300m	36.94	11.45	43.5	8.11	48.4	COHESION(21.3), LED(16.8)
	600m	47.85	11.04	29.81	11.3	58.9	LED(20.5), LSI(14.9), COHESION(14.6)
	900m	66.25	12.74	13.35	7.66	79	AI(15.5), PD(14.4)
	1,200m	51.53	17.11	25.62	5.74	68.6	PD(19.2), COHESION(18.6)
	2,400m	35.13	7.25	44.19	13.43	42.4	PLAND(20), BHR(15.6)
	4,800m	42.64	11.72	34.64	11	54.4	PLAND(49.6), AI(15.6)

and selected landscape pattern metrics were different, these studies agreed that at small scales, the effects of 3D metrics on PM pollution were higher than those of 2D metrics. It's worthwhile to note that coordination and correspondence need to be maintained between the selection of urban morphological metrics and the spatial scale. Maybe the priority scales for exploring the relationship between air pollution and 3D metrics could be controlled within 1,000 m.

Implications for Urban Planning

The "landscape pattern–air pollution" relationship studies provide valuable and practical insights for urbanists who are committed to PM mitigation. Given

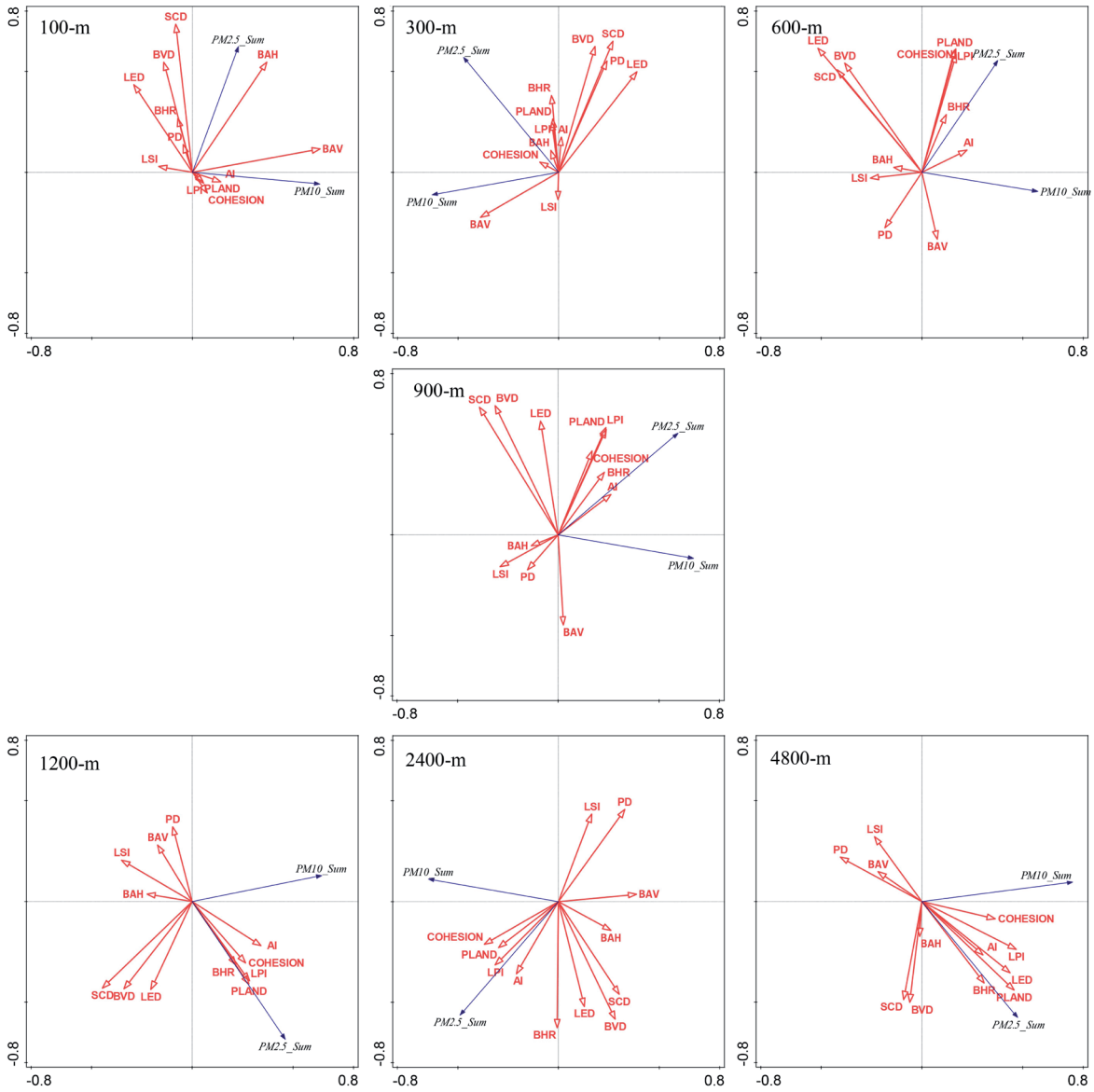

Fig. 6. The RDA biplots depicting the relationship between landscape pattern metrics (red lines) and PM pollution variables (blue lines) at distinct scales in summer.

that the dominant landscape pattern factors on PM concentrations differ greatly across seasons and scales, effective strategies to mitigate air pollution should vary as seasons and scales change. For example, during summer, when the PM concentrations were lower or at smaller scales (the buffer zones radii ≤ 1,000 m), the LED and SCD of 3D landscape pattern metrics were the key metrics that affected PM concentrations. During winter, when the PM concentrations were higher or at larger scales (2,400 and 4,800 m scales), the PLAND of 2D landscape pattern metrics was the most important explanatory variable. Then, during winter or at larger scales, a high cover of vegetation and a low cover of buildings were critical for reducing PM concentrations. By contrast, during summer or at smaller scales, the building layout should be paid more attention in terms of PM pollution mitigation. Moreover, the proportion of ecological land and building land needs to be rationally planned in urban areas. Given that urban land resources are valuable and scarce, substantially increasing ecological space and decreasing the number of artificial buildings are impractical solutions, but the horizontal expansion of artificial buildings can be replaced with a vertical extension. For example, the present study showed that the influence of building PLAND was greater than the building height metrics (e.g., BAH and BHR) on PM pollution, and then the value of building PLAND could be reduced by vertical building extension. In addition, the complex correlation of 3D landscape pattern metrics with $PM_{2.5}$ and PM_{10} implies that the relationship between the landscape pattern and PM pollutants is complicated, and morphology standards for environmental-friendly cities are not uniform [8]. For instance, the LED, SCD, and BVD were

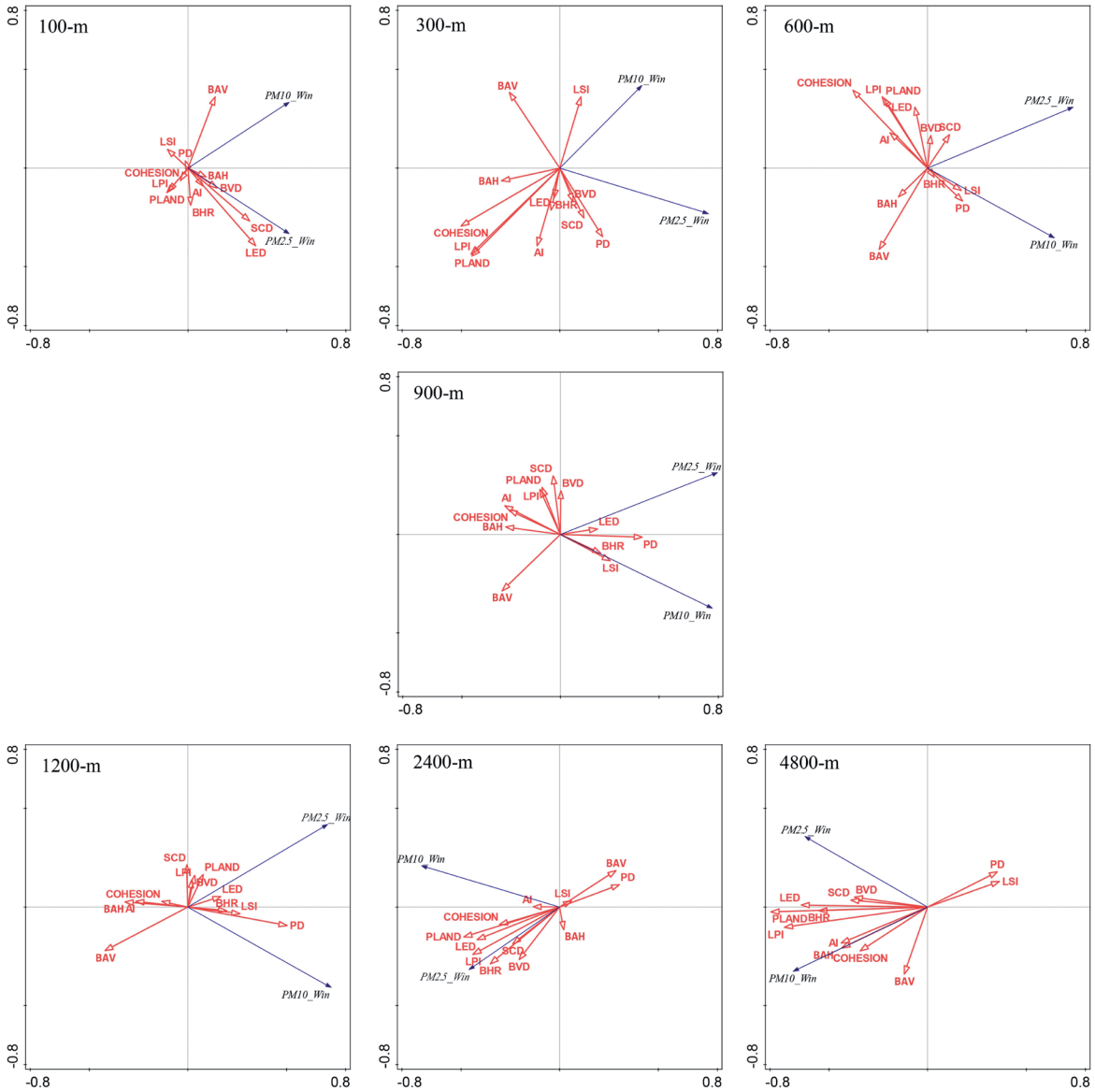

Fig. 7. The RDA biplots depicting the relationship between landscape pattern metrics (red lines) and PM pollution variables (blue lines) at distinct scales in winter.

related to relatively higher $PM_{2.5}$ concentrations but lower PM_{10} concentrations, suggesting that the diffusion and spreading of atmospheric pollutants would be either hindered or promoted by the surrounding environment. It is a practical solution to minimize the disadvantages of design principles and maximize the advantages.

Limitations

Several limitations still exist in this study: First, limited by data acquisition, some important landscape pattern metrics such as SVF have not been considered. More 2D/3D metrics could be considered for fully characterizing the landscape pattern in future works. Second, the variation of metrics across seasons was not accounted for because the landscape pattern here mainly refers to the building morphology, which may not change in a short time. Considering the variations in land cover types across different seasons, the seasonal tree morphology could be treated as supplementary characteristics of the landscape pattern. Besides, only fixed air monitoring stations were utilized in this study, which may have resulted in sup-optimal analysis due to the limited data. Future research with multiple data sources (e.g., mobile monitoring vehicles and spectral sensors) could be employed to develop high-precision and long-term studies.

Conclusions

PM pollution is a crucial and growing worldwide problem caused by urbanization, which does severe harm to public health. A multiple spatial scale analysis was established on the effects of the urban landscape pattern on PM pollution in four seasons in Nanchang,

China, via regular analysis and RDA. Six 2D and six 3D representative metrics were employed to describe the landscape pattern, and the metrics were extracted at buffer scales of 100, 300, 600, 900, 1,200, 2,400, and 4,800 m around the monitoring stations. Results showed that the effects of the urban landscape pattern on PM pollution had significant seasonal differences and spatial scale effects. The urban landscape pattern in fall and winter had a stronger influence on PM pollution than in spring and summer. The explanatory ability of metrics on PM concentrations tended to first increase, then decline, and finally increase as scales enlarge, and the highest accumulated explanatory ability was observed at the 900 m scale. At smaller scales (buffer radii ≤ 900 m), the ability of 3D metrics was stronger than 2D metrics to explain the PM concentration changes, and at larger scales (buffer radii ≥ 1,200 m), the 2D metrics were more explanatory. PLAND and COHESION were the key 2D landscape pattern metrics affecting PM pollution, and SCD and LED were the key 3D metrics. The study provided a meaningful insight into the effects of landscape patterns on PM pollution and showed the practical implications of urban air pollution mitigation, thus contributing to sustainable urban development.

Acknowledgments

This research was funded by the National Natural Science Foundation of China [Grant No. 42361015 and 62206117], Jiangxi Provincial Social Science Foundation [Grant No. 22GL46], Jiangxi Provincial University Humanities and Social Science Foundation [Grant No. JC22222]. The authors greatly appreciate the thorough review and valuable comments of the anonymous reviewer that helped improve this manuscript.

Conflict of Interest

The authors declare no conflict of interest.

References

1. LIU J., MA T., CHEN J., PENG X., ZHANG Y., WANG Y., PENG J., SHI G., WEI Y., GAO J. Insights into $PM_{2.5}$ pollution of four small and medium-sized cities in Chinese representative regions: Chemical compositions, sources and health risks. Science of The Total Environment. **918**, 170620, **2024**.
2. World Health Organization. World health statistics 2019: Monitoring health for the SDGs, sustainable development goals. World Health Organization: Geneva, Switzerland, **2019**.
3. COLLABORATORS G.B.D., ÄRNLÖV J. Global burden of 87 risk factors in 204 countries and territories, 1990–2019: a systematic analysis for the Global Burden of Disease Study 2019. The Lancet. **396** (10258), 1223, **2020**.
4. WU Y., HU J., IRFAN M., HU M. Vertical decentralization, environmental regulation, and enterprise pollution: an evolutionary game analysis. Journal of Environmental Management. **349**, 119449, **2024**.
5. CHEN T., ZHOU P., XU W., LIU Y., SUN S. Spatial-temporal evolution characteristics and influencing factors of $PM_{2.5}$ in the Yangtze River Basin. Polish Journal of Environmental Studies. **33** (2), 1611, **2024**.
6. TAO Y., ZHANG Z., OU W., GUO J., PUEPPKE S.G. How does urban form influence $PM_{2.5}$ concentrations: Insights from 350 different-sized cities in the rapidly urbanizing Yangtze River Delta region of China, 1998-2015. Cities. **98**, 102581, **2020**.
7. CAO Q., LUAN Q., LIU Y., WANG R. The effects of 2D and 3D building morphology on urban environments: A multi-scale analysis in the Beijing metropolitan region. Building and Environment. **192**, 107635, **2021**.
8. ZHANG A., XIA C., LI W. Exploring the effects of 3D urban form on urban air quality: Evidence from fifteen megacities in China. Sustainable Cities and Society. **78**, 103649, **2022**.
9. YU Y., WANG J., YU J., CHEN H., LIU V. Spatial and temporal distribution characteristics of $PM_{2.5}$ and PM_{10} in the urban agglomeration of China's Yangtze River Delta, China. Polish Journal of Environmental Studies. **28** (1), 445, **2019**.
10. LI T.Y., DENG X.J., LI Y., SONG Y.S., LI L.Y., TAN H.B., WANG C.L. Transport paths and vertical exchange characteristics of haze pollution in Southern China. Science of The Total Environment. **62**, 1074, **2018**.
11. FENG H., ZOU B., TANG Y. Scale and region-dependence in landscape-$PM_{2.5}$ correlation: Implications for urban planning. Remote sensing. **9**, 918, **2017**.
12. ZHAO X., ZHOU W., WU T., HAN L. The impacts of urban structure on $PM_{2.5}$ pollution depend on city size and location. Environmental Pollution. **292**, 118302, **2022**.
13. LEE C. Impacts of multi-scale urban form on $PM_{2.5}$ concentrations using continuous surface estimates with high-resolution in U.S. metropolitan areas. Landscape and Urban Planning. **204**, 103935, **2020**.
14. SUN J., ZHOU T., WANG D. Relationships between urban form and air quality: A reconsideration based on evidence from China's five urban agglomerations during the COVID-19 pandemic. Land Use Policy. **118**, 106155, **2022**.
15. LI F., ZHOU T. Effects of urban form on air quality in China: An analysis based on the spatial autoregressive model. Cities. **89**, 130, **2019**.
16. HUANG C., HU T., DUAN Y., LI Q., CHEN N., WANG Q., ZHOU M., RAO P. Effect of urban morphology on air pollution distribution in high-density urban blocks based on mobile monitoring and machine learning. Building and Environment. **219**, 109173, **2022**.
17. KE B., HU W., HUANG D., ZHANG J., LI X., LI C., JIN X., CHEN J. Three-dimensional building morphology impacts on $PM_{2.5}$ distribution in urban landscape settings in Zhejiang, China. Science of The Total Environment. **826**, 154094, **2022**.
18. TAN X., ZHOU Z., WANG W. Relationships between urban form and $PM_{2.5}$ concentrations from the spatial pattern and process perspective. Building and Environment. **234**, 110147, **2023**.
19. ZHAO X., ZHOU W., HAN L. The spatial and seasonal complexity of $PM_{2.5}$ pollution in cities from a social-ecological perspective. Journal of Cleaner Production. **309**, 127476, **2021**.
20. WU W., WANG Y., LIU M., LI C. A review on the use of landscape indices to study the effects of three-

dimensional urban landscape patterns on haze pollution in China. Polish Journal of Environmental Studies. **30** (4), 2957, **2021**.
21. LIU Y., CHEN C., LI J., CHEN W.Q. Characterizing three dimensional (3-D) morphology of residential buildings by landscape metrics. Landscape Ecology. **35**, 2587, **2020**.
22. WU W.B., YU Z.W., MA J., ZHAO B. Quantifying the influence of 2D and 3D urban morphology on the thermal environment across climatic zones. Landscape and Urban Planning. **226**, 104499, **2022**.
23. TIAN Y., DESOUZA P., MORA S., YAO X., DUARTE F., NORFORD L.K., LIN H., RATTI C. Evaluating the meteorological effects on the urban form-air quality relationship using mobile monitoring. Environmental Science and Technology. **56** (11), 7328, **2022**.
24. ZHOU W., TIAN Y. Effects of urban three-dimensional morphology on thermal environment: a review. Acta Ecologica Sinica. **40** (2), 416, **2020** (In Chinese).
25. YANG H.O., LENG Q.M., XIAO Y.F., CHEN W.B. Investigating the impact of urban landscape composition and configuration on $PM_{2.5}$ concentration under the LCZ scheme: a case study in Nanchang, China. Sustainable Cities and Society. **84**, 104006, **2022**.
26. YANG H.O., CHEN W.B., LIANG Z.F. Impact of land use on $PM_{2.5}$ pollution in a representative city of middle China. International Journal of Environmental Research and Public Health. **14** (5), 462, **2017**.
27. LABETSKI A., VITALIS S., BILJECKI F., ARROYO OHORI K., STOTER J. 3D building metrics for urban morphology. International Journal of Geographical Information Science. **37** (1), 36, **2023**.
28. HU C., WU W., ZHOU X., WANG Z. Spatiotemporal changes in landscape patterns in karst mountainous regions based on the optimal landscape scale: A case study of Guiyang City in Guizhou Province, China. Ecological Indicators. **150**, 110211, **2023**.
29. TAN X., ZHOU Z., WANG W. Relationships between urban form and $PM_{2.5}$ concentrations from the spatial pattern and process perspective. Building and Environment. **234**, 110147, **2023**.
30. LIOU Y.A., NGUYEN Q.V., NGUYEN K.A., VO T.H. Human-greenspace interactions with outdoor air: Landscape metric and PLS-SEM approach. Journal of Cleaner Production. **469**, 143077, **2024**.
31. LIU Y., WU J., YU D. The relationship between urban form and air pollution depends on seasonality and city size. Environmental Science and Pollution Research. **25**, 15554, **2018**.
32. PARVAR Z., MOHAMMADZADEH M., SAEIDI S. LCZ framework and landscape metrics: Exploration of urban and peri-urban thermal environment emphasizing 2/3D characteristics. Building and Environment. **254**, 111370, **2024**.
33. LI X., YANG B., XU G., LIANG F., JIANG T., DONG Z. Exploring the impact of 2-D/3-D building morphology on the land surface temperature: a case study of three megacities in China. IEEE Journal of Selected Topics in Applied Earth Observations and Remote Sensing. **14**, 4933, **2021**.
34. HUANG X., WANG Y. Investigating the effects of 3D urban morphology on the surface urban heat island effect in urban functional zones by using high-resolution remote sensing data: a case study of Wuhan, central China. Isprs Journal of Photogrammetry and Remote Sensing. **152**, 119, **2019**.
35. XU M., XU G., LI Z., DANG Y., LI Q., MIN Z., GU F., WANG B., LIU S., ZHANG Y. Effects of comprehensive landscape patterns on water quality and identification of key metrics thresholds causing its abrupt changes. Environmental Pollution. **333**, 122097. **2023**.
36. TANG J., GONG L., MA X., ZHU H., DING Z., LUO Y., ZHANG H. The oasisization process promotes the transformation of soil organic carbon into soil inorganic carbon. *Land.* **13**, 336, **2024**.
37. TIAN Y., YAO X., MU L., FAN Q., LIU Y. Integrating meteorological factors for better understanding of the urban form-air quality relationship. Landscape Ecology. **35**, 2357, **2020**.
38. MIAO C., YU S., HU Y., LIU M., YAO J., ZHANG Y., HE X., CHEN W. Seasonal effects of street trees on particulate matter concentration in an urban street canyon. Sustainable Cities and Society. **73**, 103095, **2021**.
39. SHI K., LI Y., CHEN Y., LI L., HUANG C. How does the urban form-$PM_{2.5}$ concentration relationship change seasonally in Chinese cities? A comparative analysis between national and urban agglomeration scales. Journal of Cleaner Production. **239**, 118088, **2019**.
40. ZHAO S., FENG T., TIE X., LI G., CAO J. Air pollution zone migrates south driven by East Asian winter monsoon and climate change. Geophysical Research Letters. **48** (10), e2021GL092672, **2021**.
41. SHI K., WANG H., YANG Q., WANG L., SUN X., LI Y. Exploring the relationships between urban forms and fine particulate ($PM_{2.5}$) concentration in China: a multi-perspective study. Journal of Cleaner Production, **231**, 990, **2019**.
42. ZHOU Y., YANG Y., WANG H., WANG J., LI M., LI H., WANG P., ZHU J., LI K., LIAO H. Summer ozone pollution in China affected by the intensity of Asian monsoon systems. Science of the Total Environment. **849**, 157785, **2022**.
43. POPE R., WU J. Characterizing air pollution patterns on multiple time scales in urban areas: a landscape ecological approach. Urban Ecosystems. **17**, 855, **2014**.
44. HAN L., ZHAO J., GAO Y., GU Z., XIN K., ZHANG J., Spatial distribution characteristics of $PM_{2.5}$ and PM_{10} in Xi'an City predicted by land use regression models[J]. Sustainable Cities and Society. **61**, 102329, **2020**.
45. SHI Y., LAU K.K.L., NG E. Developing street-level $PM_{2.5}$ and PM_{10} land use regression models in high-density Hong Kong with urban morphological factors. Environmental Science and Technology. **50** (15), 8178, **2016**.
46. SHI Y., XIE X., FUNG J.C.H., NG E. Identifying critical building morphological design factors of street-level air pollution dispersion in high-density built environment using mobile monitoring. Building and Environment. **128**, 248, **2018**.
47. SHI Y., REN C., LAU K.K.L., NG E. Investigating the influence of urban land use and landscape pattern on $PM_{2.5}$ spatial variation using mobile monitoring and WUDAPT. Landscape and Urban Planning. **189**, 15, **2019**.
48. MENG J., HAN W., YUAN C. Seasonal and multi-scale difference of the relationship between built-up land landscape pattern and $PM_{2.5}$ concentration distribution in Nanjing. Ecological Indicators. **156**, 111079, **2023**.
49. HU J. Synergistic effect of pollution reduction and carbon emission mitigation in the digital economy. Journal of Environmental Management. **337**, 117755, **2023**.
50. CHEN M., DAI F., YANG B., ZHU S. Effects of urban green space morphological pattern on variation of $PM_{2.5}$ concentration in the neighborhoods of five Chinese megacities. Building and Environment. **158**, 1, **2019**.